2020 IEEE/RSJ International Conference on Intelligent Robots and Systems (IROS)
October 25-29, 2020, Las Vegas, NV, USA (Virtual)

Bi-Modal Hemispherical Sensors for Dynamic Locomotion and Manipulation

Lindsay Epstein[1], Andrew SaLoutos[1], Donghyun Kim[1], and Sangbae Kim[1]

***Abstract*— The ability to measure multi-axis contact forces and contact surface normals in real time is critical to allow robots to improve their dexterous manipulation and locomotion abilities. This paper presents a new fingertip sensor for 3-axis contact force and contact location detection, as well as improvements on an existing footpad sensor through use of a new artificial neural network estimator. The fingertip sensor is intended for use in manipulation, while the footpad sensor is intended for high force use in locomotion. Both sensors consist of pressure sensing elements embedded within a rubber hemisphere, and utilize an artificial neural network to estimate the applied forces (f_x, f_y, and f_z), and contact angles (θ and ϕ) from the individual sensor element readings. The sensors are inherently robust, and the hemispherical shape allows for easy integration into point feet and fingertips. Both the fingertip and footpad sensors demonstrate the ability to track forces and angles accurately over the surface of the hemisphere ($\theta = \pm 45^\circ$ and $\phi = \pm 45^\circ$) and can experience up to 25N and 450N normal force, respectively, without saturating. The performance of the sensor is demonstrated with experimental results of dynamic control of a robotic arm with real-time sensor feedback.**

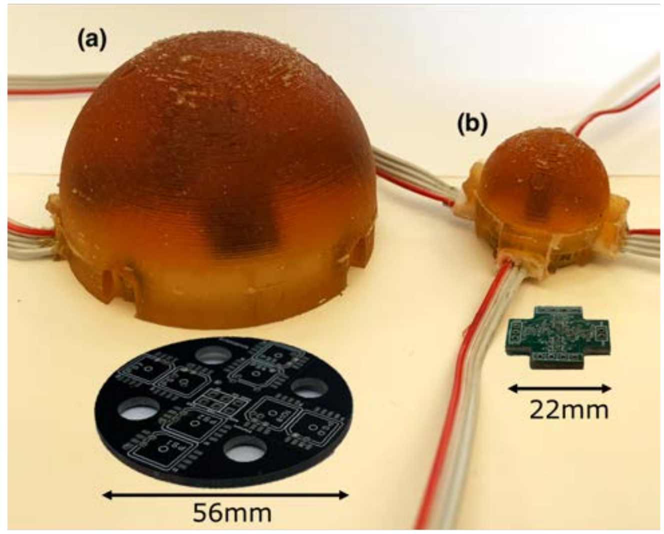

Fig. 1. **Sensor Design.** (a) Hemispherical footpad sensor and PCB. PCB shows locations of 8 piezoresisitive sensing elements in x-shaped array. (b) Hemispherical fingertip sensor and PCB. 4 cables are used in place of 1 to simplify internal routing and decrease PCB size.

I. INTRODUCTION

Humans and animals have amazing capabilities when it comes to performing dynamic physical tasks. In the wild, cheetahs can chase after prey at high speeds over varied terrain, while humans can grasp, lift, and manipulate objects of many sizes and shapes with ease. Much of this capability is related to their ability to quickly and accurately gain information about the world around them through a sense of touch [1]–[3]. Robots, in contrast, often struggle in this area. In order to be able to react to unexpected disturbances, deftly manipulate objects, and accomplish compelling feats of locomotion, robots need to be able to quickly sense information about the objects or environments they are interacting with, including contact forces and contact surface normals.

During locomotion, a better understanding of contact forces and angles can help a legged robot better understand the friction cone, or help detect and avoid slip, allowing for better, more stable, movement. However, large, dynamic robots such as the MIT Cheetah [4] require that sensors be robust to repeated impacts, insensitive to inertial noise, and able to withstand and measure high forces, up to multiple times the robot's own body weight [5]. Existing sensors are often not suitable for these conditions. Conventional force/torque sensors, for example, are very stiff and include fragile strain gauges which may break under high impacts when used in the limbs of legged robots. They also tend to be heavy, expensive, and prone to inertial noise. Other tactile sensing technologies use a variety of methods including measuring pressure or flow [6]–[8], electrical properties [9], [10], or optics [11], [12] to measure forces and contact locations. These sensors tend to be designed for much smaller force ranges than are experienced in locomotion, and often do not measure contact location and forces along three axes simultaneously.

For manipulation, information about the contact locations and contact forces can allow robots to achieve more stable grasps. Towards this goal, many more tactile sensors have been developed. These include piezoresistive, capacitive, optical, and barometric based sensors. However, many do not provide information on both normal and tangential forces, as well as contact location, are sensitive to vibration related noise, or lack physical robustness [13]. Another example is Gelsight [14]–[16], which provides extremely detailed information about the surface being contacted by using a camera and 3D surface reconstruction. Gelsight has enabled robotic manipulators to estimate and improve the quality of their grasps, but requires a camera inside each sensor, making it less robust to high impact forces, and has a higher computational cost to process the data to infer contact information.

For more dynamic tasks that require fast sensing and

[1]Authors are with the Biomimetic Robotics Laboratory at the Department of Mechanical Engineering, Massachusetts Institute of Technology (MIT), Cambridge, MA, 02139, USA. lepstein@mit.edu

mechanical durability, Chuah et. al. developed a bi-modal sensor that measures the contact location as well as normal and shear forces while being robust to impacts [17]. This work introduces a novel fingertip sensor intended to address the need for contact and force measurement in a smaller form factor. It also introduces a new artificial neural network (ANN) estimator for use with both the existing footpad sensor [17] and the novel fingertip sensor.

Both sensor designs utilize barometric pressure sensors embedded within a rubber hemisphere to sense contact forces in 3 axes and contact locations for quasi-point contact. For the footpad sensor, the new regression process using an artificial neural network was tested and compared with the previous Gaussian process regression method. Using the ANN regression, a contact normal tracking task and a slip detection task were carried out using a three degree-of-freedom robotic arm, the results of which are presented here. The fingertip sensor utilizes the same concept of stress field force and contact angle sensing as the footpad sensor but scales it down to a form factor and force range that can be used in grippers for more reliable manipulation. Both sensors are robust, low cost, and capable of accurately and simultaneously measuring forces and contact location.

The paper is organized as follows. The design and fabrication of both sensors is described in Section II. The data collection setup is covered in Section III. Sections IV and V discuss the training and testing of two estimators for the sensors, as well as the experimental results using both of these estimators. Section VI presents two applications in which the footpad sensor is attached to a robotic arm, and Section VII details future work and ongoing improvements in the development of these sensors.

II. Hemispherical Footpad Design and Fabrication

This paper presents two versions of a sensor based on the principle of stress field force sensing – one intended for high force applications such as locomotion, and one intended for lower force applications such as manipulation. As described by Chuah et. al. [17]–[20], stress field force sensing is a method in which pressure sensors embedded in a rubber exterior sample the stress distribution within that rubber at discrete locations. The output measurements from these pressure sensors are then used to reconstruct the unique contact forces and contact location on the surface of the rubber for quasi-point contact.

The overall fabrication process for both sensors is similar and follows the procedure developed by Chuah et. al. [17]–[20]. In both sensors, eight barometric pressure sensors and associated electronics are soldered onto a printed circuit board (PCB). The PCB is then embedded within a hard polymer and a hemisphere of polyurethane rubber. The resulting sensor is durable and well protected from the external environment. Fig. 1 shows both PCBs and sensor designs.

TABLE I
SENSOR CHARACTERISTICS

	Footpad Sensor	Fingertip Sensor
Pressure Sensing Element	MPXH6400A	BMP388
PCB Diameter	43.2 mm	17.8 mm
Final Sensor Diameter	56 mm	22 mm
Force Range	2 - 450N	0.5 - 25N
Sampling Rate	1kHz	200Hz

A. Footpad Sensor Design

The footpad sensor (Fig. 1a) is intended for use in high force applications in which robust 3-axis force and contact location detection is necessary, such as locomotion. Towards this goal, the sensor is mechanically robust, insensitive to inertial noise, able to withstand high forces without failure, and able to provide contact and force information at a high rate.

The design of the footpad sensor is the same as that described by Chuah et al. [17].

The overall sensor is 56mm in diameter, has a maximum sampling rate of 1 kHz, and can experience a maximum normal force of 450N applied at the center of the sensor ($\theta = \phi = 0^\circ$) without saturating.

B. Fingertip Sensor Design

The fingertip sensor (Fig. 1b) is significantly smaller, and is intended for use in lower force applications in which the same information about forces and contact location is beneficial, such as manipulation. The sensor is particularly suited to integration into fingertips for manipulation due to its small size, hemispherical, fingertip-like form factor, lower force range, and high sensitivity (< 0.5N).

It follows the same general design of that of the footpad sensor, but with new sensing components and a modified PCB design to allow for the smaller form factor.

Some key changes in the fabrication process that allow for development of the new, smaller fingertip sensor include:

- New piezoresisitive sensing element
- Method of covering the sensing elements during polymer molding using folded transparency sheets
- Modification to the mounting insert size and location

This sensor utilizes eight BMP388 barometric pressure sensors (Bosch Sensortec), which have a pressure range of 300-1250 hPa, a footprint of 2x2mm, and a maximum sampling rate of 200 Hz. These digital sensors utilize SPI communication and do not require an additional on-board ADC. The barometric pressure sensors are arranged on the PCB in the same x-shaped array as in the footpad sensor.

The overall fingertip sensor is 22mm in diameter, has a maximum sampling rate of 200 Hz, and can experience a maximum normal force of 25N at location $\theta = \phi = 0^\circ$ before hitting saturation.

The different properties of the footpad and fingertip sensors are summarized in Table I.

Fig. 2. **Experimental Setup.** (a) A CNC mill setup is used to collect asterisk and roll data. The sensor is mounted on the mill in place of a spindle, brought in contact with a force/torque sensor, and driven through a number of pre-programmed paths. (b) An IMU is mounted on top of the sensor to provide ground truth contact location information when collecting handheld data. The IMU mount also serves as a handle to allow for easy manual manipulation of the sensor through unstructured paths. (c) The contact location on the hemispherical surface is defined by sequential rotations about the x and y axes of the sensor of angles θ and ϕ, respectively. At each contact location, the shear forces f_x and f_y are defined locally as being tangent to the spherical surface, while the normal force f_z is defined to be orthogonal.

III. Data Collection Setup

Training and validation datasets were collected for both hemispherical sensors using two different data collection setups, seen in Figure 2.

In the first, a modified 3-axis CNC milling machine (MicroMill DSLS 3000 from MicroProto Systems) was used to control the position and motion of the sensor. The machine was modified to allow for rotation about the x axis of the mill through the addition of a trunnion table and about the z axis of the mill through the addition of a manual rotation stage. This setup is the same as that described by Chuah et. al. [17]–[20]. It was used to collect two separate datasets - an asterisk dataset, which was used to train the sensor, and a roll dataset, which was used to test the sensor performance.

A separate setup was used to collect the handheld dataset. This setup utilized the same force/torque sensor (ATI Delta SI-660-60 from ATI Industrial Automation) for ground truth force data as in the mill setup, but added an integrated IMU (3DM-CX5-25 AHRS from MicroStrain) mounted on top of the footpad or fingertip sensor to provide ground truth contact location information without use of the mill. This data was collected and logged using Visual Studio C++. The transition to C++ allows for real-time estimation through integration of the neural network evaluation into the data processing code using the frugally deep library[1] and eases the transition onto a microcontroller (Sec. VI).

A. Asterisk Data

For the asterisk dataset, data was collected at multiple contact locations across the hemispherical surface. At each test point, the hemispherical sensor was compressed against the force/torque sensor, then driven along an asterisk-shaped path on the force/torque sensor surface at increasing compression levels. Asterisk data was collected for contact locations in the range $\theta = -45°$ to $\theta = 45°$ and $\phi = -45°$ to $\phi = 45°$. Force and angle conventions can be seen in Fig. 2c. Forces are defined such that shear forces f_x and f_y are tangent to the rubber hemisphere surface, and the normal force f_z is perpendicular to the hemispherical rubber surface. θ and ϕ are defined as sequential explicit rotations about the x and y axis, respectively.

[1]https://github.com/Dobiasd/frugally-deep

B. Roll Data

To represent "rolling" contact that a footpad or fingertip could undergo during locomotion or manipulation, the roll dataset was used. For this dataset, the sensor was compressed against the force/torque sensor to a set level at various fixed rotations about the z axis. The force/torque sensor was then "rolled" along the surface of the sensor using the mill's trunnion table. For the fingertip roll dataset, the compression level was decreased part-way through rolling to prevent the sensor from saturating.

C. Handheld Data

A handheld dataset was also collected to test the sensor performance. In generating the handheld dataset, the output from the IMU acted as a ground truth for contact location as the sensor was manipulated against the force/torque sensor by hand, rather than by the mill, to provide a more organic set of forces and contact locations.

IV. Force and Angle Estimators

Two different methods of estimating the contact forces and location from the readings of the eight pressure sensors are investigated for both the footpad and fingertip sensors. In both methods, the estimator is trained using a combined dataset consisting of the asterisk data and one set of handheld data. It is then evaluated on two new datasets - the unseen roll dataset and a separate, unique handheld dataset.

Before training or testing the estimators, the force data from the force/torque sensor is filtered using a convolutional filter to eliminate high frequency noise due to the motion

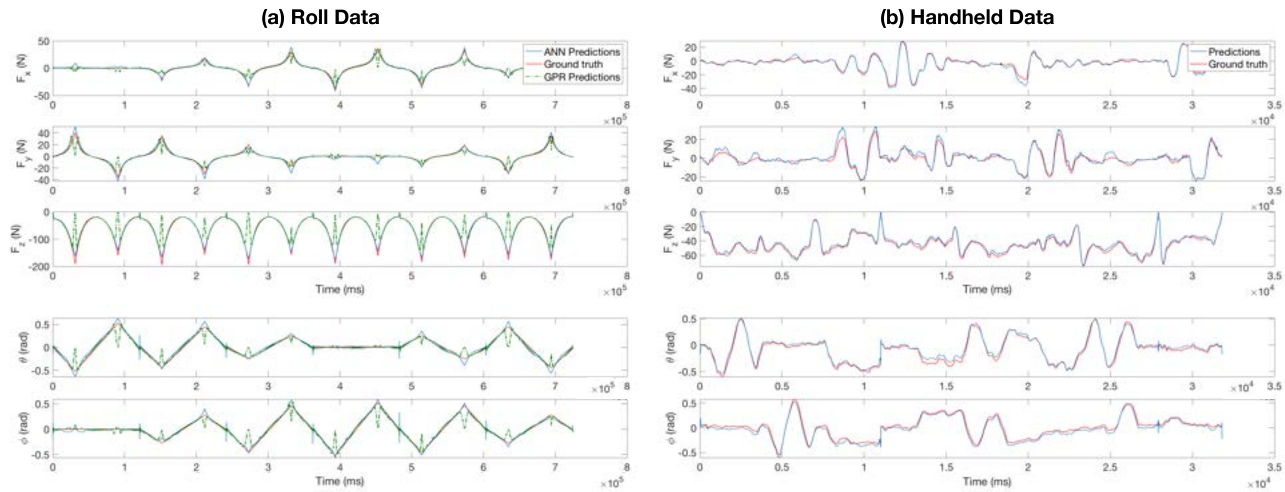

Fig. 3. **Footpad Sensor ANN and GPR Results** (a) Contact force and angle ANN estimations are plotted versus ground truth data for the roll dataset. They are very closely aligned, even in regions outside the force range of the training dataset. Some spikes are seen in the angle estimation when the normal force is very low. For the GPR estimator, all five outputs match well with the ground truth below 120N normal force, but deviate significantly in the range $f_z \gtrsim$ 120N. (b) Results for the handheld dataset. ANN predicted output closely tracks the ground truth, including on an unstructured dataset.

TABLE II
FOOTPAD SENSOR PERFORMANCE

	Asterisk Data			Roll Data			Handheld Data		
Artificial Neural Network									
	RMSE (N)	Norm. RMSE (%)	R^2(%)	RMSE (N)	Norm. RMSE (%)	R^2(%)	RMSE (N)	Norm. RMSE (%)	R^2(%)
f_x	1.937	1.330	0.974	1.921	2.564	0.959	1.883	2.901	0.964
f_y	2.078	1.407	0.971	2.677	3.484	0.926	2.656	5.057	0.911
f_z	2.717	1.397	0.994	4.175	2.151	0.990	2.327	3.130	0.964
θ	0.092	5.852	0.941	0.040	3.859	0.963	0.040	3.644	0.972
ϕ	0.098	6.193	0.942	0.028	2.679	0.983	0.045	3.978	0.953
Gaussian Process Regression									
f_x	1.051	0.722	0.993	4.263	5.689	0.801	1.327	2.044	0.982
f_y	0.919	0.622	0.995	4.435	5.772	0.797	2.224	4.235	0.938
f_z	2.086	1.079	0.996	31.279	16.314	0.464	1.147	1.595	0.991
θ	0.027	1.709	0.995	0.076	7.264	0.871	0.026	2.385	0.988
ϕ	0.035	2.190	0.992	0.077	7.286	0.875	0.034	3.009	0.973

of the mill. This filtering was not implemented in previous work [17].

A. Gaussian Process Regression

The first method investigated is Gaussian process regression (GPR) [21]. In GPR, the equation:

$$\hat{y}_j = \mathbf{k}_* \left(\boldsymbol{K} + \sigma_n^2 \boldsymbol{I}\right)^{-1} \mathbf{y}_j, \tag{1}$$

is used to estimate the scalar output $\hat{y}_j$ (estimated f_x, f_y, f_z, θ, or ϕ) from the input vector $\mathbf{x}$, which is comprised of the eight analog pressure readings ($\begin{bmatrix} s_1, & s_2, & \cdots, & s_8 \end{bmatrix}^\top$). Because this equation produces a scalar output it must be calculated five times – once for each output being estimated. This method was used previously to train and evaluate the original footpad sensor design; in-depth implementation details and variable definitions can be found in [17].

GPR performs well for training and testing the sensor on $1/8^{th}$ of the hemisphere surface [17]. However, as the number of training data points increases to cover the full surface of the hemisphere, the computation time of GPR increases exponentially. This is due to the large matrix inversion and multiplication in Eq. (1), as well as the fact that all five outputs must be solved for individually.

B. Artificial Neural Network Estimator

An artificial neural network (ANN) is also investigated. The goal of this approach is to offer an alternative to GPR that is faster, able to handle larger training datasets, and more robust to unseen data.

The structure of the ANN used for both the footpad and fingertip sensors is as follows: the eight pressure sensor reading inputs $\begin{bmatrix} s_1, & s_2, & \cdots, & s_8 \end{bmatrix}$ are connected to a layer of 12 neurons. These neurons are fully connected to a hidden layer of 25 neurons, which are then fully connected to an output layer that predicts the five outputs $\begin{bmatrix} f_x, & f_y, & f_z, & \theta, & \phi \end{bmatrix}$. The neurons in each layer use the activation functions ReLU,

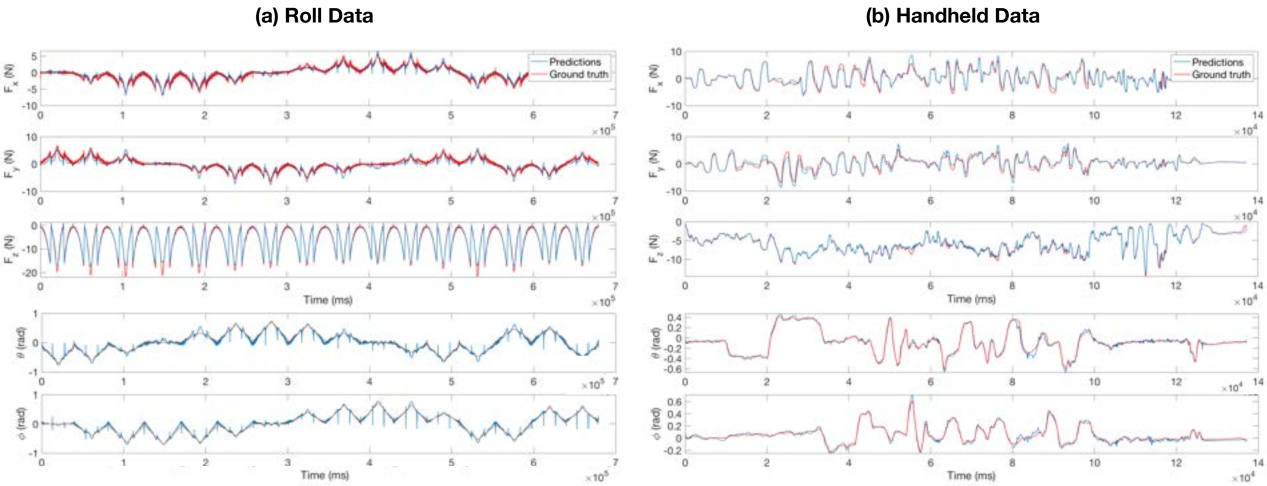

Fig. 4. **Fingertip Sensor ANN Results** Similar to the footpad sensor, for both test datasets the ANN estimation very closely follows the ground truth forces and contact angles for the fingertip sensor. (a) Roll data results. (b) Handheld data results.

TABLE III
FINGERTIP SENSOR PERFORMANCE

	Artificial Neural Network								
	Asterisk Data			Roll Data			Handheld Data		
	RMSE (N)	Norm. RMSE (%)	R^2(%)	RMSE (N)	Norm. RMSE (%)	R^2(%)	RMSE (N)	Norm. RMSE (%)	R^2(%)
f_x	0.678	2.272	0.956	0.601	4.650	0.915	0.697	4.960	0.929
f_y	0.884	3.052	0.926	0.832	6.183	0.840	0.730	5.621	0.876
f_z	0.382	1.918	0.986	0.662	2.866	0.984	0.299	2.148	0.985
θ	0.123	7.814	0.903	0.058	4.138	0.964	0.027	2.596	0.985
ϕ	0.099	6.297	0.945	0.050	3.561	0.976	0.024	2.894	0.964
	Gaussian Process Regression								
f_x	0.582	1.950	0.968	1.649	12.815	0.218	0.790	5.663	0.907
f_y	0.610	2.104	0.965	1.801	13.437	0.087	1.194	9.296	0.665
f_z	0.350	1.768	0.986	3.010	13.027	0.674	0.368	2.573	0.979
θ	0.042	2.700	0.988	0.083	5.950	0.913	0.039	3.778	0.967
ϕ	0.043	2.757	0.989	0.093	6.670	0.901	0.028	3.332	0.952

ELU, and Sigmoid, respectively, and the ANN is trained in Keras [2] with a Tensorflow backend. Training is completed with the Adam optimizer and a mean squared error cost function.

In addition to filtering, all input and output data is scaled to the range [0,1] before being used to train and test the ANN. Because the final layer of the ANN uses a sigmoid activation function, the outputs of the ANN automatically fall on the range [0,1]. These outputs are then re-scaled to their final values using the initial scaling parameters (i.e. maximum and minimum values) from the training data.

V. RESULTS

When evaluated on the asterisk dataset, roll dataset, and handheld dataset, the footpad and fingertip sensors are found to have comparable performance. While the GPR estimator outperforms the ANN on the training data, the new ANN estimator is found to generalize better to unseen data, particularly to unsee data outside the force range of the training data. For this reason, as well as the training dataset size limitations of GPR, the ANN is selected as the primary estimator when evaluating both footpad and fingertip sensor performance.

The root mean squared error (RMSE) and coefficient of determination R^2 are used as metrics to quantify the performance of the GPR estimator and the ANN estimator on the asterisk, roll, and handheld datasets.

A. Footpad

The results for the footpad sensor with the ANN estimator are shown in Fig. 3. For both test datasets, there is a very close match between the predicted outputs and the ground truth values for f_x, f_y, f_z θ, and ϕ. In Fig. 3a some discrete spikes can be seen in the ANN estimations of θ, and ϕ. These occur when the normal force is very low, as the sensor has difficultly estimating contact location when there is little or no contact being made. These deviations were included when calculating RMSE and R^2 values.

[2]https://keras.io/

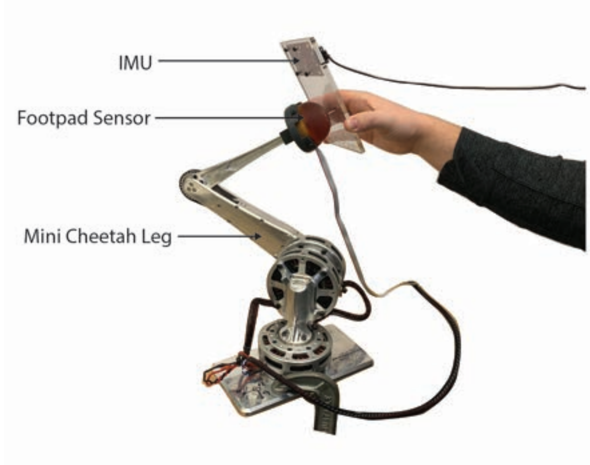

Fig. 5. **Contact Tracking Application** Experimental setup for the constant force contact location tracking application. The footpad sensor is mounted on the end of a modified Mini Cheetah leg, which then uses the contact location estimate from the footpad sensor to follow a manually manipulated block of plastic. An IMU mounted on the block allows for evaluation of the sensor performance.

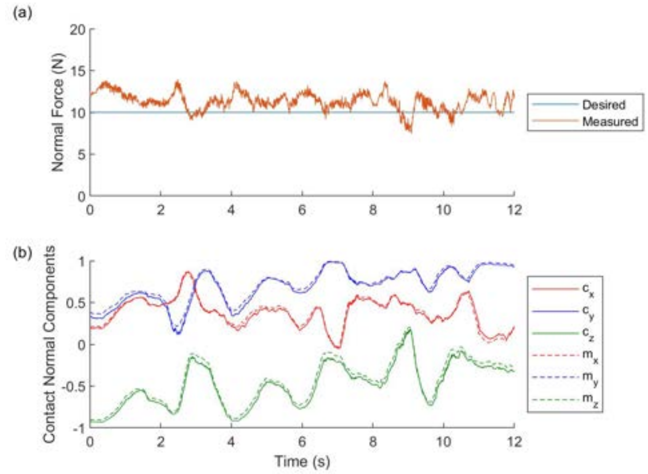

Fig. 6. **Contact Tracking Sample Data** Sample of collected data for the contact tracking application. (a) Estimated normal force and desired (constant) normal force. (b) Components of the estimated contact normal (c_x, c_y, c_z) and the measured components from the IMU (m_x, m_y, m_z).

The corresponding RMSE, normalized RMSE, and R^2 values, as well as a comparison to the GPR estimator performance on all three datasets, can be seen in Table II. As mentioned previously, the GPR estimator outperforms the ANN on the training dataset, however it performs significantly worse than the ANN when generalizing to data outside of the force range of the training set, such as that seen in the roll dataset. The high error in the GPR estimate outside of the force range of the training dataset can be seen in Fig. 3a, where the GPR estimated forces deviate significantly from the ground truth when $f_z \gtrsim 120$N. This cutoff is likely caused by the training data distribution, which fell primarily below this force range. This was not seen in previous experiments with GPR [17] as the force range of the previous test datasets did not exceed that of the previous training dataset.

B. Fingertip

The results for the fingertip sensor ANN estimator are shown in Fig. 4. Similar to the footpad sensor results, there is a very close agreement between the predicted outputs and the ground truth values for f_x, f_y, f_z, θ, and ϕ for both test datasets. This demonstrates that the overall sensor and estimator design is scalable and can function across multiple sizes and force ranges. As with the footpad sensor data, some spikes can be seen in the estimations of θ and ϕ when there is little or no contact being made with the surface. These could likely be avoided by filtering the angle estimation output.

Table III shows the RMSE, normalized RMSE, and R^2 values for all three datasets, as well as a comparison to the GPR estimator performance on the same datasets. The ANN has lower RMSE and higher R^2 values than the GPR for all five outputs for both evaluation datasets, indicating superior performance and better generalization to unseen data.

VI. Application

To further validate the sensor performance a footpad sensor was attached at the end of a single leg of the MIT Mini Cheetah [22], which had been previously repurposed as a three degree-of-freedom arm [23]. A microcontroller (Nucleo-64 STM446RE) was used to collect data from the footpad sensor, evaluate the neural network to determine the contact forces and angles, and send control commands to the three motors of the arm over a CAN bus. Using this test system, two simple applications of the sensors were explored. Video of the testing can be found in the supplementary material.

A. Tracking and Maintaining Contact

For the first application, the robot end-effector was commanded to exert a constant 10N force normal to the sensor surface at the contact point. The contact normal vector was calculated in the world frame from the estimated sensor contact angles and the robot's joint angles. In order to increase the accuracy of the rendered force at the end-effector, torques for compensating the weight of the robot arm and sensor were added. To measure the true contact normal, the same IMU used for the handheld data collection was mounted on a block of plastic and used to contact the sensor. Since the sensor's estimate of normal force was not used in the control loop, it was used to measure how accurately the system was tracking the desired force. The arm with the mounted sensor and the IMU plate can be seen in Fig. 5. For this application, data was collected and plotted from the IMU and the arm at 250 Hz.

Fig. 6a shows the normal force measurements from the sensor as well as the commanded normal force. Fig. 6b shows the contact normal as calculated from the sensor readings and robot kinematics compared to the normal vector as tracked by the IMU. The normal force is only roughly tracked,

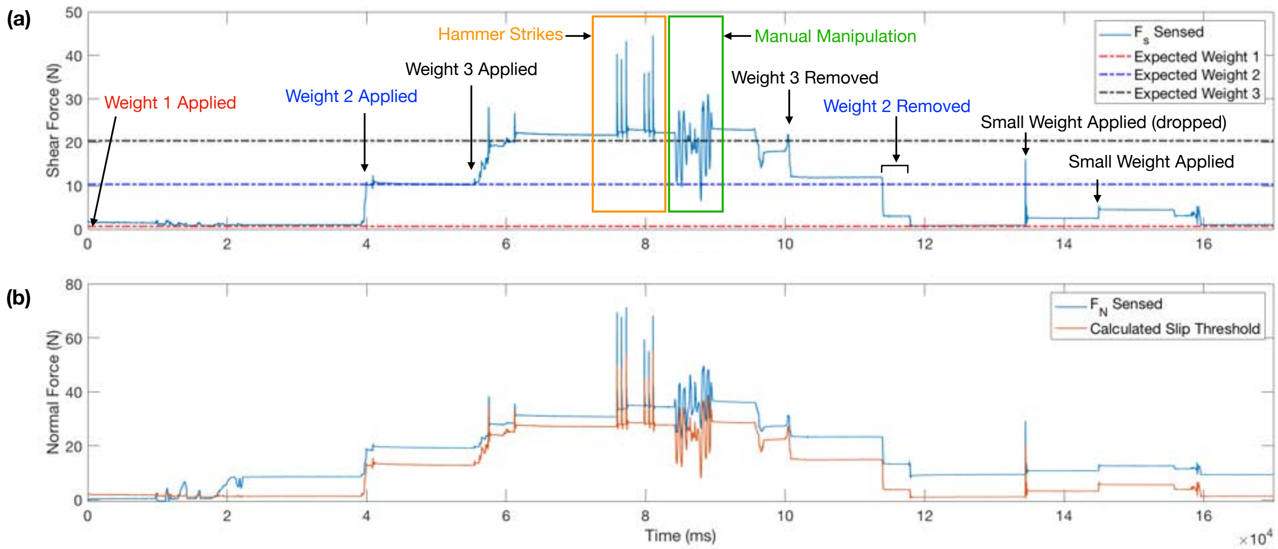

Fig. 7. **Slip Detection and Prevention Sample Data** Sample of collected data for the slip detection and prevention application. (a) Measured shear force, labeled with important testing events. The expected shear force for the larger added weights are also shown. (b) Measured normal force and calculated minimum normal force to avoid slip. The calculated slip threshold is found by dividing the measured shear force by $\mu = 0.8$.

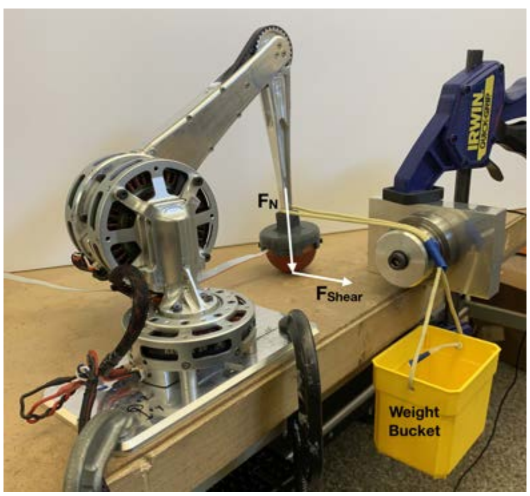

Fig. 8. **Slip Detection and Prevention Application** Experimental setup for the slip detection and prevention application. The footpad sensor's estimation of the applied shear force is used to calculate the normal force required to prevent the sensor from slipping on the table surface.

and could be improved by compensating for motor non-linearities (e.g. friction, cogging) as well as remaining in a "quasi-static" regime when moving the contact surface. More importantly, the components of the contact normal vector are very accurate to the ground truth provided by the IMU. This results in a qualitatively stable demonstration in which the end-effector appears to "stick" strongly to the contact surface, as seen in the supplementary video.

B. Slip Detection and Prevention

For the second application, the shear and normal force measurements were used to detect and prevent slip at the robot end-effector. To begin, the robot was commanded to exert a small normal force of 5N directly into the table surface. A bucket was attached to the lower limb of the arm and suspended over the corner of the table. This setup can be seen in Fig. 8. The coefficient of friction between the table and the sensor surface was estimated as $\mu = 0.8$. Using this coefficient of friction, the controller modulated the commanded normal force such that the sensed shear force was within the friction cone by a small buffer amount. As a result, the controller would not exert unnecessarily large normal forces for small values of shear force and would not apply so little force as to let the arm slip.

During testing, two groups of weights added to the bucket resulted in approximately 10N steps in the shear force measured by the sensor. After the weights were added, the sensor base was hit with a hammer in order to induce large, rapid spikes in the shear force. Shear force was also manually applied at the sensor base in various directions. The weights were then unloaded in the reverse order. Finally, smaller weights were added and removed to show that the sensor maintains good resolution even at lower force magnitude.

In Fig. 7a, the measured shear force is plotted along with the expected measurements from each of the large weights. The shear measurements track the expected values well and also show the high-frequency oscillations due to the impacts of the dropped weights and the hammer. In Fig. 7b, the measured normal force is shown along with the calculated slip threshold. The normal force is successfully controlled such that it is always above the slip threshold, even in the case of the sudden high-magnitude hammer impacts and the manual loading, thereby detecting and preventing slip.

VII. Discussion and Conclusion

A. Discussion and Future Work

Both the footpad and fingertip sensors demonstrate the ability to simultaneously and in real time determine contact location and measure forces along three axes. Due to the sensor design and the nature of stress field force sensing, both sensors are low cost, robust, insensitive to inertial noise, high-bandwidth, and have a hemispherical shape for easy integration on to point feet or fingertips.

Overall, the newly developed ANN estimator outperforms the GPR estimator for both the footpad and fingertip sensors. The ANN demonstrates better generalization to unseen data, is faster and less computationally intense than the GPR, and is not limited in the amount of training data it can utilize. The footpad sensor with ANN estimator also demonstrates the ability to successfully implement surface normal following and slip detection and prevention in real time (up to 1kHz).

Future work on these sensors will include testing the footpad sensor on the MIT Cheetah [4] and integrating the fingertip sensor into a robotic gripper to further evaluate performance. It will also include further streamlining the sensor fabrication processes to make them more repeatable, and working to characterize and quantify key properties of the sensors including precision, durability, and drift over time. Future improvements to the sensors could also include investigating alternate sensing element arrangements, such as inclining the pressure sensing elements or changing their locations, to increase the active sensing area or improve performance.

B. Conclusion

This paper presents a new fingertip sensor for 3-axis contact force and contact location detection as well as a new ANN estimator that improves performance of the existing footpad sensor. Both sensors demonstrate the ability to accurately sense applied shear and normal forces, as well as contact location for quasi-point contact. The bi-modal capability of the footpad sensor is further demonstrated through two applications. First, the footpad sensor is used on a robot arm to track a block using contact location estimation, and second, the sensor is used to detect and prevent slip at its surface.

These sensors are inherently robust and low cost, and have the potential to greatly expand the capabilities of robots in both locomotion and manipulation.

Acknowledgments

The authors would like to thank Meng Yee (Michael) Chuah, Benjamin Katz, Jiaheng Zhang, Ellen O'Connell and Bernardo Aceituno for their assistance with this work.

References

[1] G. Robles-De-La-Torre, "The importance of the sense of touch in virtual and real environments," *IEEE MultiMedia*, vol. 13, no. 3, pp. 24–30, 2006.

[2] J. Monzée, Y. Lamarre, and A. M. Smith, "The Effects of Digital Anesthesia on Force Control Using a Precision Grip," *Journal of Neuroscience*, vol. 89, no. 2, pp. 672–683, 2003.

[3] P. Jenmalm and R. S. Johansson, "Visual and Somatosensory Information about Object Shape Control Manipulative Fingertip Forces," *Journal of Neuroscience*, vol. 17, no. 11, pp. 4486–4499, 1997.

[4] G. Bledt, M. J. Powell, B. Katz, J. Di Carlo, P. M. Wensing, and S. Kim, "MIT Cheetah 3: Design and Control of a Robust, Dynamic Quadruped Robot," in *IEEE/RSJ International Conference on Intelligent Robots and Systems*. IEEE, 2018, pp. 2245–2252.

[5] M. Y. M. Chuah, "Design principles of multi-axis, large magnitude force sensors based on stress fields for use in human and robotic locomotion," Ph.D. dissertation, Massachusetts Institute of Technology, 2018.

[6] Y. Tenzer, L. P. Jentoft, and R. D. Howe, "The feel of mems barometers: Inexpensive and easily customized tactile array sensors," *IEEE Robotics Automation Magazine*, vol. 21, no. 3, pp. 89–95, Sep. 2014.

[7] J. W. Guggenheim, L. P. Jentoft, Y. Tenzer, and R. D. Howe, "Robust and inexpensive six-axis force–torque sensors using mems barometers," *IEEE/ASME Transactions on Mechatronics*, vol. 22, no. 2, pp. 838–844, April 2017.

[8] S. E. Navarro, O. Goury, G. Zheng, T. M. Bieze, and C. Duriez, "Modeling Novel Soft Mechanosensors Based on Air-Flow Measurements," *IEEE Robotics and Automation Letters*, vol. 4, no. 4, pp. 4338–4345, 2019.

[9] T. P. Tomo, S. Somlor, A. Schmitz, L. Jamone, W. Huang, H. Kristanto, and S. Sugano, "Design and characterization of a three-axis hall effect-based soft skin sensor," *Sensors*, vol. 16, no. 4, 2016.

[10] Z. Su, K. Hausman, Y. Chebotar, A. Molchanov, G. E. Loeb, G. S. Sukhatme, and S. Schaal, "Force estimation and slip detection/classification for grip control using a biomimetic tactile sensor," in *IEEE-RAS 15th International Conference on Humanoid Robots (Humanoids)*. IEEE, 2015.

[11] J. S. Heo, J. H. Chung, and J. Lee, "Tactile sensor arrays using fiber bragg grating," *Sensors and Actuators*, vol. 126, p. 312–327, 2006.

[12] M. Ohka, H. Kobayashi, J. Takate, and Y. Mitsuya, "Sensing Precision of an Optical Three-axis Tactile Sensor for a Robotic Finger," in *IEEE International Conference on Robot and Human Interactive Communication*. IEEE, 2006.

[13] Kappassov, Z., Corrales, J.A., and Perdereau, V., "Tactile sensing in dexterous robot hands — Review," *Robotics and Autonomous Systems*, vol. 74, pp. 195–220, 2015.

[14] W. Yuan, S. Dong, and E. H. Adelson, "Gelsight: High-resolution robot tactile sensors for estimating geometry and force," *Sensors*, vol. 17, no. 12, 2017.

[15] D. Ma, E. Donlon, S. Dong, and A. Rodriguez, "Dense tactile force distribution estimation using gelslim and inverse fem," in *International Conference on Robotics and Automation*. IEEE, 2019.

[16] E. Donlon, S. Dong, M. Liu, E. Adelson, and A. Rodriguez, "GelSlim: A High-Resolution, Compact, Robust, and Calibrated Tactile-sensing Finger," in *International Conference on Robotics and Automation*. IEEE, 2018.

[17] M. Y. M. Chuah, L. Epstein, D. Kim, J. Romero, and S. Kim, "Bi-Modal Hemispherical Sensor: A Unifying Solution for Three Axis Force and Contact Angle Measurement," in *IEEE/RSJ International Conference on Intelligent Robots and Systems*. IEEE, 2019, pp. 7968–7975.

[18] M. Y. M. Chuah, M. Estrada, and S. Kim, "Composite Force Sensing Foot Utilizing Volumetric Displacement of a Hyperelastic Polymer," in *IEEE/RSJ International Conference on Intelligent Robots and Systems*. IEEE, 2012, p. 67.

[19] M. Y. M. Chuah and S. Kim, "Enabling Force Sensing During Ground Locomotion: A Bio-Inspired, Multi-Axis, Composite Force Sensor Using Discrete Pressure Mapping," *IEEE Sensors Journal*, vol. 14, no. 5, pp. 1693–1703, May 2014.

[20] M. Y. M. Chuah and S. Kim, "Improved normal and shear tactile force sensor performance via Least Squares Artificial Neural Network (LSANN)," in *International Conference on Robotics and Automation*. IEEE, 2016.

[21] C. E. Rasmussen and C. K. I. Williams, *Gaussian Processes for Machine Learning*. MIT Press, Jan. 2006.

[22] B. Katz, J. Di Carlo, and S. Kim, "Mini cheetah: A platform for pushing the limits of dynamic quadruped control," in *International Conference on Robotics and Automation*. IEEE, 2019, pp. 6295–6301.

[23] B. G. Katz, "A low cost modular actuator for dynamic robots," Master's thesis, Massachusetts Institute of Technology, 2018.